A Novel Synthetic Loading Method for Multiple Three-phase Winding Electric Machines

Mikel Zabaleta, Emil Levi, *Fellow*, *IEEE*, and Martin Jones

***Abstract*—The paper develops a version of the synthetic loading method, suitable for testing of multiphase machines with multiple three-phase distributed windings. The method is at first discussed in general terms for a structure with k three-phase stator windings (i.e. total number of phases is $n = 3k$). Subsequent detailed development is described for a dual three-phase (six-phase) stator winding configuration. With a control architecture that allows the use of half of the three-phase windings as a motor and the other half as a generator, the machine (and/or the converter) can be tested under full rated power without the need for any mechanical load. Moreover, the power consumed from the grid is in essence equal only to the total losses of the system. Modelling, based on the double *d-q* approach, and the control layout that includes full cross-coupling decoupling are described for a permanent magnet (PM) synchronous machine. An experimental test rig with a double three-phase PM machine of 150 kW rating is detailed and the samples of experimental results are provided to verity the theoretical considerations.**

***Index Terms*—Electric machines, multiple three-phase winding machines, synthetic loading, full-power testing.**

I. Introduction

The traditional arrangement to test rotating machines (especially in the MW region) is the so called back-to-back method [1]. This requires two rotating machines with their shafts mechanically coupled and one power converter connected to each of the machines. One of them will operate as the motor controlling the speed of the shaft while the other will be acting as a generator thus introducing a braking torque in the shaft. With this arrangement, the machine and/or the converter can be tested up to full rated power and only the supply of the power losses of all the devices (predominantly machines, transformers and converters) is required. Although all these components usually have high efficiencies, around 96%, an 8-10 MW back-to-back arrangement will have overall losses above 800 kW (since the actual power managed would be 16-20 MW). It should be noted that the machine tested using two-machine back-to-back method in [1] is an asymmetrical six-phase machine, with 30 degrees shift between the two three-phase windings.

A significant drawback of the back-to-back arrangement is the necessity to have two machines, two converters and usually two power transformers and switchgear. All these components lead to a significant expenditure on the testing facility and, additionally, increase the required footprint, which also translates into a further cost.

In order to avoid the drawbacks of the back-to-back testing method, the synthetic loading has been proposed as an alternative method to obtain the efficiency and heat rise of a three-phase machine, while requiring a reduced set of equipment components. This idea, although rather old [2], became feasible with the advent of PWM inverters and was predominantly developed and used in conjunction with induction motors [3-6]. In a nutshell, synthetic loading means that the mechanical load is not required and different operating conditions of the machine under test, including rated current operation and rated temperature rise, are normally achieved by introducing a pulsating torque (by means of current harmonic injection) at a frequency high enough so that the speed of the machine hardly varies due to inertia. The same principle of machine testing has been further used for testing of synchronous machines with field winding [7] and, in more recent times, in relation to permanent magnet synchronous machines of different types [8-10].

As far as the three-phase machines are concerned, the choice is limited and one can opt for either the back-to-back method or for the synthetic loading. However, when it comes to testing of multiphase machines, a new opportunity opens up. In particular, if an n-phase machine is built using k windings with a phases each, and the neutral points of the windings are isolated, it becomes possible to devise a combined synthetic back-to-back method for the testing, which preserves good features of the synthetic loading test (no requirement for the mechanical coupling with another machine) while also eliminating the main drawback of the back-to-back method, the need for two machines. The concept is based on the fact that, in an n-phase machine, individual a-phase windings can be operated in different regimes, with different powers processed. Such an idea was for the first time introduced in [11], for an asymmetrical six-phase (dual three-phase) induction machine with connection to two different electric sources, a fuel cell stack and a battery. Hence there are two independently controlled three-phase inverters (a=3, k=2, n=6) and powers processed by them can be varied, including even the change of the direction of the power flow: one winding can generate and charge the battery, while the other winding motors and provides power for propulsion/generation.

The concept described above has gained much more interest in very recent times and is typically associated with either multi-source electric vehicles or with dc microgrids [12-17]. In all the available reports the basic winding is a three-

Manuscript received November 23, 2017; revised March, 02 2018; accepted May 03, 2018.

The authors would like to acknowledge the Windpower R&D Department of Ingeteam Power Technology for supporting this research work.

M. Zabaleta is with the Windpower R&D Department of Ingeteam Power Technology, Sarriguren, 31621 Spain (mikel.zabaleta@ingeteam.com).

E. Levi and M. Jones are with the Liverpool John Moores University, Faculty of Engineering and Technology, Liverpool L3 3AF, U.K. (e.levi@ljmu.ac.uk, m.jones2@ljmu.ac.uk).

phase one (a=3), while the number of them, k, differs and typically takes values of 3 and 4, in addition to the already mentioned k=2. The other major difference relates to the modelling approach used to arrive at an appropriate control structure.

Multiple d-q modelling approach has been utilised in [11, 12] to develop arbitrary power sharing between winding sets of asymmetrical 6-phase and 12-phase machines, respectively. The advantage of this modelling approach is that the information on individual winding set d-q currents is directly available, so that current references for arbitrary power sharing are formulated in a simple manner. However, multiple d-q approach leads to heavy cross-coupling between equations of individual winding sets, which require compensation in the control system. This is a drawback of this technique (the other shortcoming, not relevant for this discussion, is the absence of unique harmonic mapping property). Power sharing using the alternative, vector space decomposition (VSD) modelling approach has been discussed in [13-15, 17]. In this case the complete electromechanical energy conversion process takes place in the first (d-q) plane of the multidimensional space, regardless of the phase number and regardless of the number of three-phase sub-windings in the machine. The impedance in all the other (x-y) planes is governed by stator resistance and stator leakage inductance. Hence the information on individual three-phase winding d-q currents (and thus powers as well) is lost. To achieve power sharing when VSD is used as the starting point, one actually has to formulate non-zero current references in the x-y plane(s) in order to enable redistribution of the power between three-phase sub-windings. In [13, 14] the sharing is examined for an asymmetrical 12-phase machine with four neutral points and the current references in x-y planes are formulated by solving the stator current vector equations, while focusing on minimizing their magnitudes. Nine-phase machines of induction and synchronous type are discussed in [15, 16], respectively. In [15] VSD is used as the starting point but it is then combined with the multiple d-q approach to formulate appropriate current references in the x-y plane(s) for the required power sharing pattern, while [16] reverts back to using again the multiple d-q modelling approach (also known as multi-stator). Asymmetrical six-phase machine is yet again covered in [17], using VSD approach as the starting point and then formulating x-y current references in a manner similar to [15] (i.e. a combined VSD and multiple d-q approach).

Regardless of the recent relatively high interest in the power sharing capability of multiphase machines with a multitude of three-phase windings, the applicability of this approach in devising a testing method for the said machines is restricted to only [18, 19]. In this two-part work the authors applied the concept of power sharing to the back-to-back testing system of a 12-phase machine, with full characteristics of the synthetic loading method. In particular, two three-phase windings were paralleled to the same inverter and operated in motoring, while the other two were similarly connected to the second inverter and operated in generating mode. The structure of the machine considered in [18, 19] made the implementation of the control algorithm rather simple, since the 12-phase (quadruple three-phase) fractional-slot PM machine, with concentrated windings, was considered. As a consequence of this construction, there is no coupling between different three-phase windings, meaning that the machine behaves as four separate three-phase machines with common rotor and the shaft.

In this paper, the alternative testing arrangement of [18, 19] is extended to machines with distributed windings, where the coupling between individual three-phase windings is strong. It is particularly well-suited to machines with an even number (k=2,4,6…) of a-phase windings, since then one half of the a-phase windings operates as a motor while the other half behaves as a generator (thus emulating the mechanical load). With this arrangement, only half of the components compared to the classic back-to-back testing method are required. Also, there is no need for a separate loading machine, so that synthetic loading is achieved through regenerative operation of half of the machine's windings. An illustration of the classical back-to-back arrangement and the one discussed here is shown in Fig. 1a and Fig. 1b, respectively. The machine considered here is with n=6, a=3, k=2.

The paper is organised as follows. Section II provides a summary of the control structure used in the testing. Section III describes the experimental set-up and gives the experimental results, while section IV concludes the paper.

II. Control Architecture

In order to be able to operate some windings of the machine as a motor (with positive q-axis currents) and others

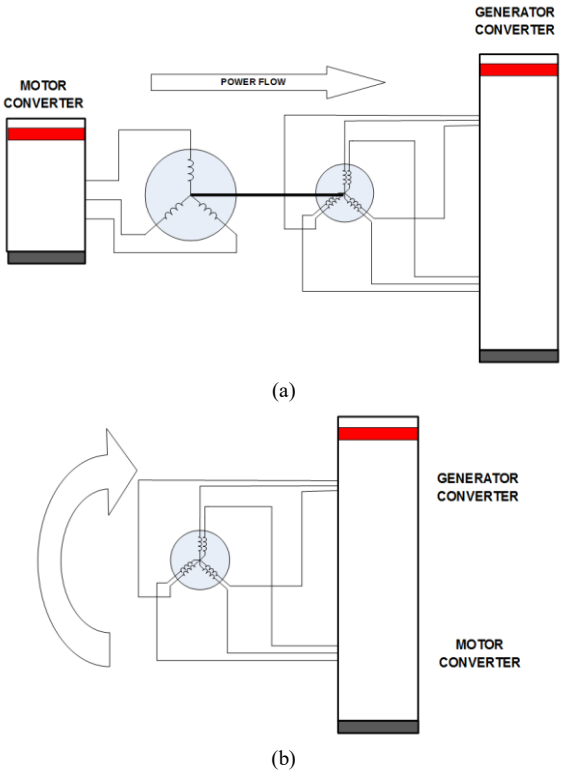

Fig. 1. Back-to-back test arrangement (a) and the alternative arrangement suitable for multiphase machines with k windings with a phases each (b) (case with k=2, a=3 is shown).

as generator (with negative q-axis currents), a control architecture that facilitates the operation of the machine with unequal current sharing is required. While both VSD and multiple d-q approach can be used for the control system development, the selected one here is the latter approach. The main reason for using multiple d-q approach is that it requires hardly any change in the control software. This is so since this approach uses two sets of current regulators (one for each three-phase winding). In fact, the only modification needed resides in the way the q-axis current references are calculated for each current regulator set. The downside of it is, as already mentioned, that the control system must include some decoupling terms that help transform the initial multiple-input multiple-output (MIMO) model with heavy cross-couplings into a set of decoupled single-input single-output (SISO) models. The procedure to obtain these decoupling terms can be found in [20] for an asymmetrical six-phase asynchronous machine and it is adapted here to a permanent magnet synchronous machine. A detailed description of the control architecture as well as a current regulator tuning procedure can be found in [21] and only a summary is provided in what follows.

A. Machine Model

In general, the modelling of an n-phase permanent magnet synchronous machine is very similar to that of a three-phase machine, with the only difference in the dimension of the domain. To start with, the equation of the stator's voltages in the natural (phase-variable) domain can be expressed as

$$[v_s]_{abc} = [R_s]_{abc} \cdot [i_s]_{abc} + \frac{d[\Psi_s]_{abc}}{dt} \tag{1}$$

where the dimensions of the voltage ($[v_s]_{abc}$), current ($[i_s]_{abc}$) and flux vectors ($[\Psi_s]_{abc}$) are nx1 and the resistance matrix ($[R_s]$) is nxn and diagonal in form. The equation of the flux linkages can be written as

$$[\Psi_s]_{abc} = [L_s]_{abc} \cdot [i_s]_{abc} + [\Psi_{PM}]_{abc} \tag{2}$$

where $[L_s]_{abc}$ represents the stator inductance matrix and $[\Psi_{PM}]_{abc}$ the flux provided by the permanent magnets.

The multiple d-q modelling approach consists in splitting the multiphase machine into several three-phase systems and applying to each of them at first the well-known three-phase Clarke's decoupling transformation, with an appropriate phase shift angle for each three-phase system,

$$[T_3(\alpha)] = \frac{2}{3}\begin{bmatrix} \cos(\alpha) & \cos\left(\alpha+\frac{2\pi}{3}\right) & \cos\left(\alpha+\frac{4\pi}{3}\right) \\ \sin(\alpha) & \sin\left(\alpha+\frac{2\pi}{3}\right) & \sin\left(\alpha+\frac{4\pi}{3}\right) \\ \frac{1}{2} & \frac{1}{2} & \frac{1}{2} \end{bmatrix} \tag{3}$$

where α can take values of 0, $\pi/6$, and $2\pi/6$ for a dual three-phase (six-phase) machine, considered further on.

Application of (3) to the equations (1) and (2), and subsequent transformation into the common synchronously rotating reference frame lead to the resultant model that can be expressed in state-space representation as

$$\begin{aligned} [\dot{X}] &= [A] \cdot [X] + [B] \cdot [u] \\ [Y] &= [X] \end{aligned} \tag{4}$$

$$[X] = [i_{d1} \;\; i_{q1} \;\; i_{d2} \;\; i_{q2}]^T$$
$$[u] = [v_{d1} \;\; v_{q1} \;\; v_{d2} \;\; v_{q2}]^T$$

where

$$[A] = \begin{bmatrix} a_{11} & a_{12} & a_{13} & a_{14} \\ a_{21} & a_{22} & a_{23} & a_{24} \\ a_{13} & a_{14} & a_{11} & a_{12} \\ a_{23} & a_{24} & a_{21} & a_{22} \end{bmatrix}$$

$$[B] = \begin{bmatrix} g_{d11} & 0 & g_{d12} & 0 \\ 0 & g_{q11} & 0 & g_{q12} \\ g_{d12} & 0 & g_{d11} & 0 \\ 0 & g_{q12} & 0 & g_{q11} \end{bmatrix}$$

and

$$\begin{aligned} a_{11} &= -g_{d11} \cdot r_s \\ a_{12} &= g_{d11} \cdot \omega_r \cdot \left(L_{ls} + \frac{3}{2} \cdot L_{mq}\right) + g_{d12} \cdot \omega_r \cdot \frac{3}{2} \cdot L_{mq} \\ a_{13} &= -g_{d12} \cdot r_s \\ a_{14} &= g_{d11} \cdot \omega_r \cdot \frac{3}{2} \cdot L_{mq} + g_{d12} \cdot \omega_r \cdot \left(L_{ls} + \frac{3}{2} \cdot L_{mq}\right) \\ a_{21} &= -g_{q11} \cdot \omega_r \cdot \left(L_{ls} + \frac{3}{2} \cdot L_{md}\right) - g_{q12} \cdot \omega_r \cdot \frac{3}{2} \cdot L_{md} \\ a_{22} &= -g_{q11} \cdot r_s \\ a_{23} &= -g_{q11} \cdot \omega_r \cdot \frac{3}{2} \cdot L_{md} - g_{q12} \cdot \omega_r \cdot \left(L_{ls} + \frac{3}{2} \cdot L_{md}\right) \\ a_{24} &= -g_{q12} \cdot r_s \end{aligned}$$

$$\begin{aligned} g_{d11} = g_{d22} &= \frac{2 \cdot L_{ls} + 3 \cdot L_{md}}{2 \cdot L_{ls} \cdot (L_{ls} + 3 \cdot L_{md})} \\ g_{d12} = g_{d21} &= \frac{-3 \cdot L_{md}}{2 \cdot L_{ls} \cdot (L_{ls} + 3 \cdot L_{md})} \\ g_{q12} = g_{q21} &= \frac{-3 \cdot L_{mq}}{2 \cdot L_{ls} \cdot (L_{ls} + 3 \cdot L_{mq})} \\ g_{q11} = g_{q22} &= \frac{2 \cdot L_{ls} + 3 \cdot L_{mq}}{2 \cdot L_{ls} \cdot (L_{ls} + 3 \cdot L_{mq})} \end{aligned}$$

The system's cross-couplings become evident in the matrix $[A]$ of (4). This matrix has non-zero elements in all the positions, indicating a heavy cross-coupling. This is the same model property as in the case of an induction machine [20]. Finding the frequency response of the obtained state-space model, illustrated in Fig. 2, the cross-couplings appear again in the form of gain peaks relating every input (voltage) with every output (stator current) at the rotating speed of the rotor (50 Hz in this case). This cross-coupled behaviour makes the attainment of high dynamic responses in the current loops very difficult. This is so since the operation of the current regulator in one axis of one stator winding gets reflected as a perturbation in all the other axes of the machine. In order to avoid this limitation, a decoupling strategy is required.

B. Cross-coupling Decoupling

From Fig. 2, two different cross-couplings can be identified. Taking the $d1$-axis as a reference (the first row of Fig. 2), the first cross-coupling appears with the inputs v_{q1}, v_{q2}, indicating that the voltages in the $q1$- and $q2$-axes influence the current in the $d1$- and $d2$-axes. This cross-coupling is the same that appears in a three-phase machine and is usually referred to as d-q cross-coupling. Secondly, the input v_{d2} also has an influence on i_{d1} and this cross-coupling will be referred to as stator-stator cross-coupling. Additionally, there appears the third cross-coupling related to the inputs matrix $[B]$, as it is

not diagonal in form. This cross-coupling will be referred to as inputs cross-coupling. Applying a state-feedback decoupling, a feedback matrix to virtually cancel each of the *d-q*, the stator-stator, and inputs cross-couplings can be found. The corresponding state-feedback matrices ($[K_{dq}]$, $[K_{st}]$ and $[K_{in}]$, respectively) for a permanent magnet synchronous machine with double three-phase windings result in the following form, respectively [21]:

$$[K_{dq}] = \begin{bmatrix} 0 & k_{d1} & 0 & k_{d2} \\ k_{q1} & 0 & k_{q2} & 0 \\ 0 & k_{d2} & 0 & k_{d1} \\ k_{q2} & 0 & k_{q1} & 0 \end{bmatrix}$$

with

$$\begin{aligned} k_{d1} &= -\omega_r \cdot \left(L_{ls} + \frac{3}{2} \cdot L_{mq}\right) \\ k_{d2} &= -\omega_r \cdot \frac{3}{2} \cdot L_{mq} \\ k_{q1} &= \omega_r \cdot \left(L_{ls} + \frac{3}{2} \cdot L_{md}\right) \\ k_{q2} &= \omega_r \cdot \frac{3}{2} \cdot L_{md} \end{aligned} \quad (5)$$

$$[K_{st}] = \begin{bmatrix} k_{st1} & 0 & k_{st2} & 0 \\ 0 & k_{st3} & 0 & k_{st4} \\ k_{st2} & 0 & k_{st1} & 0 \\ 0 & k_{st4} & 0 & k_{st3} \end{bmatrix}$$

with

$$\begin{aligned} k_{st1} &= -\frac{{g_{d12}}^2}{{g_{d11}}^2 - {g_{d12}}^2} \cdot r_s \\ k_{st2} &= \frac{g_{d11} \cdot g_{d12}}{{g_{d11}}^2 - {g_{d12}}^2} \cdot r_s \\ k_{st3} &= -\frac{{g_{q12}}^2}{{g_{q11}}^2 - {g_{q12}}^2} \cdot r_s \\ k_{st4} &= \frac{g_{q11} \cdot g_{q12}}{{g_{q11}}^2 - {g_{q12}}^2} \cdot r_s \end{aligned} \quad (6)$$

$$[K_{in}] = \begin{bmatrix} k_{in1} & 0 & k_{in2} & 0 \\ 0 & k_{in3} & 0 & k_{in4} \\ k_{in2} & 0 & k_{in1} & 0 \\ 0 & k_{in4} & 0 & k_{in3} \end{bmatrix}$$

with

$$\begin{aligned} k_{in1} &= \frac{g_{d11}}{{g_{d11}}^2 - {g_{d12}}^2} \\ k_{in2} &= -\frac{g_{d12}}{{g_{d11}}^2 - {g_{d12}}^2} \\ k_{in3} &= \frac{g_{q11}}{{g_{q11}}^2 - {g_{q12}}^2} \\ k_{in4} &= -\frac{g_{q12}}{{g_{q11}}^2 - {g_{q12}}^2} \end{aligned} \quad (7)$$

By incorporating all these decoupling terms (5)-(7) into the control structure, the machine model gets fully decoupled in each of the axes, transforming the initial MIMO model into several SISO models. In Fig. 3 it can be seen how, after including the decoupling terms, the frequency response exhibits a predominantly diagonal functional dependence (note the scaling of the vertical axes), indicating that the control of each of the states (i_{d1}, i_{q1} and i_{d2}, i_{q2} currents) is governed mainly by its input (v_{d1}, v_{q1} and v_{d2}, v_{q2}, respectively).

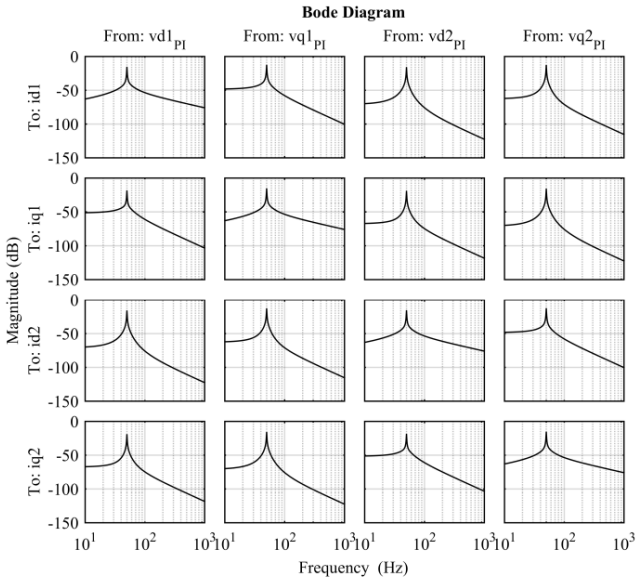

Fig. 2. Frequency response of the machine's equations transformed following the multiple *d-q* approach. A rotation at 50 Hz has been considered.

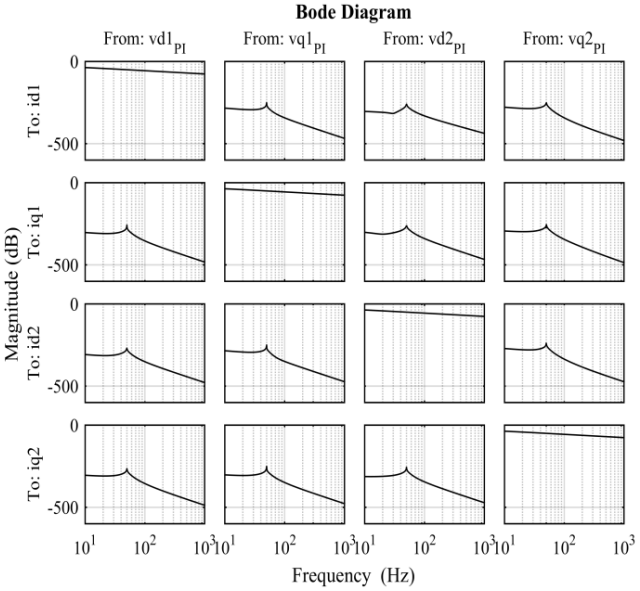

Fig. 3. Frequency response of the machine's equations transformed following the multiple *d-q* approach and with all the decoupling terms applied. A rotation at 50 Hz has been considered.

Impact of the three types of cross-coupling, described with (5)-(7), on the machine's quality of operation has been examined using both simulation and the experimental setup (described shortly). This is believed to be important since, as noted already, it is these cross-couplings that make the control significantly more involved than in [18, 19], because decoupling has to be used. The results of these studies, where simulation and experimental testing was done always i) with full set of decoupling terms according to (5)-(7), and ii) with one of the three sets of decoupling terms removed, can be summarised as follows. Cross-coupling described with (6) is the least important one and its impact on the system operation is rather small in the tested machine. Compensation of this cross-coupling could have been therefore omitted.

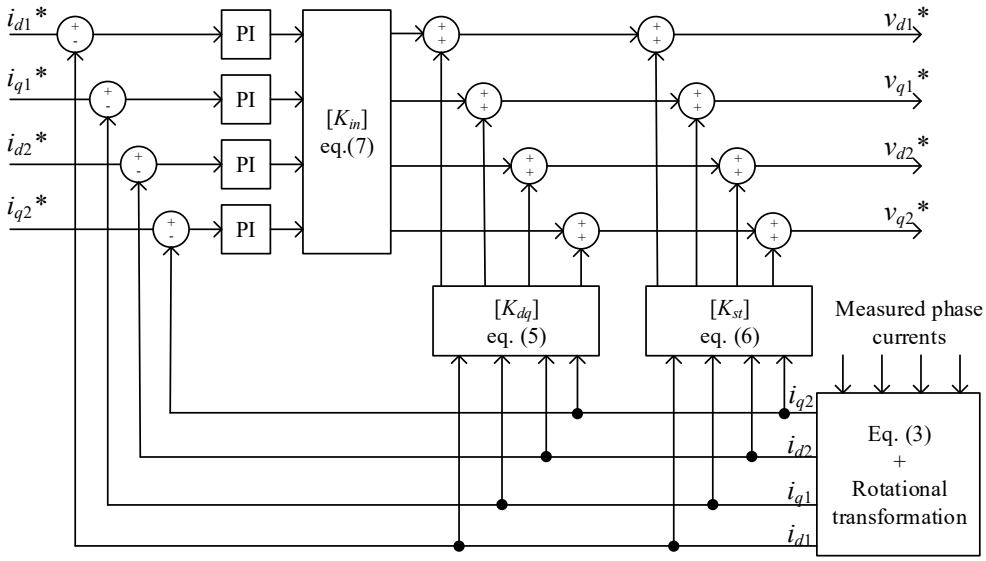

Fig. 4. Current regulator structure including decoupling terms.

On the other hand, cross-couplings described with (5) and (7) affect significantly the dynamics and hence their compensation is mandatory. In the testing described in the next section all three sets of decoupling terms are used. An illustration of the applied current control is shown in Fig. 4.

III. Experimental Results

A. Experimental Rig

The test bench used for this research is the test rig where Ingeteam emulates (at a reduced scale) the behaviour of offshore wind converters [22]. The test rig has three machine arrangements to cater for the three electrical machines already used in wind turbines (i.e. electrically excited synchronous machine, asynchronous machine and permanent magnet machine). Each of the machine arrangements consist of a 150kW dc machine that normally acts as a motor regulating the rotational speed and the ac machine under test, as seen in Fig. 5a. In the tests reported here the dc machine is mechanically connected but is not powered; hence the total losses of the system include mechanical losses of the dc machine (this is an unavoidable limitation of the test rig). The test rig is equipped with full set of measurement sensors, thus enabling recording of various currents and powers. It further also includes two 150 kW, 690 V conversion lines (Fig. 5b), each of which is composed of two three-phase three-level IGBT-based NPC converters arranged in back-to-back configuration for the connection to the machine and the grid. Conversion line data are summarised in Table I. At the machine side, the powers are measured directly at the windings (i.e. prior to the machine-side converters), while at the grid side power measurements are taken at the grid terminals (i.e. after the grid-side converters).

For the purposes of the tests described further on, the machine arrangement containing a double three-phase PM machine (zero spatial displacement between two three-phase windings) was used. Each of the three-phase windings of the permanent magnet machine, rated at 75 kW, 690 V, is connected to a conversion line. Machine data and parameters are given in Table II. It should be noted that the various inductance values in Table II are not those originally provided by the machine manufacturer, since those have been found to be inaccurate. Hence, a parameter identification procedure, detailed in [22], has been devised and the inductance values obtained in this way are listed in Table II.

The conversion lines are equipped with the same controllers as in the converters for real-world applications, so that the results obtained here can be directly extrapolated to the real operational scenarios. The current controller structure is as shown in Fig. 4 and it therefore includes full cross-coupling decoupling. Details of the procedure used to tune current controllers can be found in [21]. The NPC converters at both the machine side and the grid side are switched at 800 Hz. Machine's phase current is limited to 45 Arms.

Table I. Conversion Line Parameters

Conversion line	
Parameter	Value
ac voltage	690 – 1380 V
dc bus voltage	1050 – 2300 V
Maximum current	125 A
IGBT dead time	10 µs
IGBT minimum ON time	15 µs
Switching frequency	600-6000 Hz

Table II. Machine Data and Parameters

PM Machine	
Data / Parameter	Value
Pole pairs	8
Rated Power	150 kW (75 kW per winding)
d-axis magnetising inductance (L_{md})	1.081 mH
q-axis magnetising inductance (L_{mq})	1.176 mH
Leakage inductance (L_{ls})	1.054 mH
Phase winding resistance (R_s)	76.9 mΩ
Nominal frequency (f_n)	66.6 Hz
No-load line-to-line voltage (V_0) at f_n	751 V
Nominal line-to-line voltage (V_n)	690 V
Number of phases (n)	6
Shift angle (σ)	0

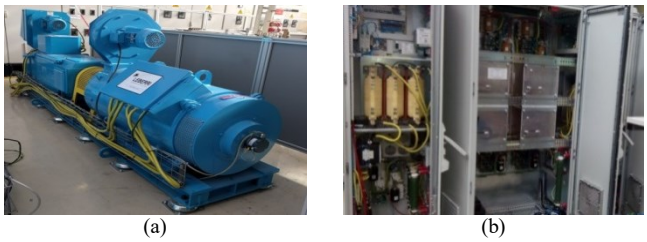

(a) (b)

Fig. 5. Electrical machine arrangement (a) and conversion line with back-to-back NPC converter arrangement (b).

In the experimental rig, the first three-phase winding (W1) operates in the motoring mode, thus following the speed and voltage commands. Hence, W1 is speed-controlled and the latter sets the *d*-axis current command. The second winding (W2) is operated as a generator, by varying its *q*-axis current command while keeping the *d*-axis current at zero (unless specified differently). Winding W2 is hence torque-controlled. Results presented further on have been extracted directly from the Ingeteam test platform, where the following conventions for positive power flow apply: at the machine side, motoring convention governs positive power flow, while at the grid side the positive power is for generating convention[1].

B. Dynamics of Power Sharing - Test Results

In the initial steady state W2 is under no-load condition, while W1 handles the total losses of the machine (including dc motor's mechanical losses), approximately 1.85 kW. The machine rotates at 300 rpm. A torque command, equivalent to 5 kW step, is then applied to W2. The top plot in Fig. 6 shows the power handled by each of the three-phase windings of the machine (black trace applies to W2, while the grey one is for W1). The bottom plot shows the power handled by the grid side converters associated to each of the winding (again, black trace is for W2 while the grey trace is for W1).

As can be seen from the upper plot in Fig. 6, W1 initially caters for the machine losses, while W2 operates with zero power. Upon application of the step in torque command to W2, which corresponds to 5 kW step, W2 goes into generation mode reaching around 4.6 kW in approximately 0.5 s. Simultaneously, W1 intake of power increases and, in final steady state, it corresponds to the sum of W2 power and the machine (including dc driving machine) losses (around 6.6 kW). Of course, at the grid side (bottom plot in Fig. 6) total losses include the losses in the converters, meaning that the total power delivered to the grid (W2 power, black trace) is around 3.15 kW, while the total power taken by W1 is approximately 9.33 kW (grey trace).

In the next test at 300 rpm W2 generates 10 kW. A step in the W2 generating torque is then applied, such that the W2 power changes from 10 kW to 18 kW. Powers of the two windings are shown in the top plot of Fig. 7.

The lower plot in Fig. 7 shows the net power on the grid side (in essence, the negative value of the total system losses). It can be seen how, as the change of the generating braking torque is very fast, the net power absorbed is firstly reduced until the speed regulator starts reacting and increasing the absorbed W1 power leading to the final steady state value.

Fig. 8 shows another set of experimental results, collected again at 300 rpm under steady-state operating conditions, with the developed testing method. The machine was handling a total power of 43 kW, with W1 consuming 23 kW in motoring mode and W2 generating 20 kW (top plot). The net total power consumption of only approximately 8 kW was recorded at the grid side (lower plot). This includes all the losses of the machine under testing, the losses of the machine-side and grid-side converters, and also the mechanical losses of the dc (driving) machine, which was not mechanically disconnected during the tests (as noted already).

In the tests reported so far *d*-axis current of W2 was held at zero, while *d*-axis current of W1 was set by the voltage controller. As a consequence, currents in the two three-phase windings are significantly different. An illustration is shown in Fig. 9, for operating frequency of 50 Hz and peak *q*-axis current in the generating winding equal to 60 A.

Since machine testing may also involve temperature rise evaluation in addition to efficiency measurement, as discussed in [18, 19], it is desirable to operate the three-phase windings with phase currents that are as close in values as possible. Hence, in the results presented in the next subsection, the phase currents of W1 and W2 have been near-equalised by using redistribution of the *d*-axis currents of W1 and W2.

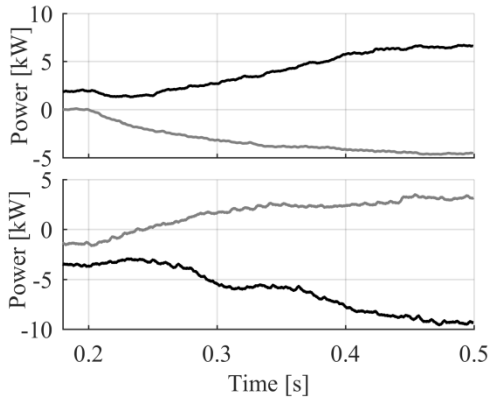

Fig. 6. Power handled by the converters of each of the three-phase windings at 300 rpm (grey trace for W1, black for W2) when a step command of 5 kW is applied at t = 0.2 s to the W2. The top plot shows powers at the machine-side converters while the bottom plot shows powers at the grid side.

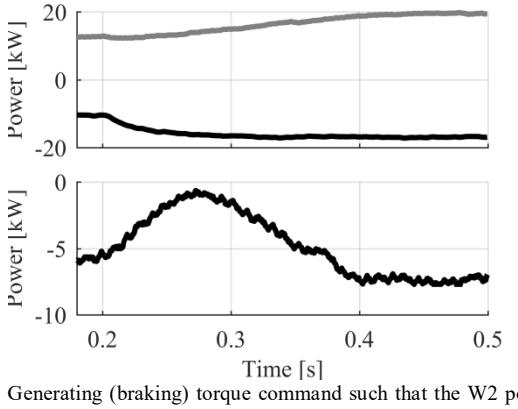

Fig. 7. Generating (braking) torque command such that the W2 power steps from 10 kW to 18 kW at 300 rpm. The top plot shows the power handled by each of the windings (grey trace for W1, black for W2). The bottom plot shows the net power delivered to the grid (negative value of the total losses).

[1] The authors decided to retain this notation, which leads to negative total loss values, since it gives the true information about the rig operation.

C. Steady-state Losses and Efficiency - Test Results

For the purposes of total loss and efficiency evaluation, the phase currents of the two windings have been equalised by introducing the negative *d*-axis current into W2 as well. This led to a reduction in the W1 *d*-axis current, dictated by the voltage controller, and enabled operation with basically the same currents in W1 and W2. The applied procedure can be explained by means of the machine's model, shown in (4), from which the inductance matrix

$$L_s = \begin{bmatrix} L_{sd} & 0 & 0 & 1.5L_{md} & 0 & 0 \\ 0 & L_{sq} & 0 & 0 & 1.5L_{mq} & 0 \\ 0 & 0 & L_{ls} & 0 & 0 & 0 \\ 1.5L_{md} & 0 & 0 & L_{sd} & 0 & 0 \\ 0 & 1.5L_{mq} & 0 & 0 & L_{sq} & 0 \\ 0 & 0 & 0 & 0 & 0 & L_{ls} \end{bmatrix} \quad (8)$$

can be obtained. It shows that the stator flux seen by each of the windings is dependent on the currents in both windings. This means that one can vary the amplitude of the flux seen by winding W1 (governed by the first row in (8)) with the *d*-axis current of winding W2 through the $(3/2)L_{md}$ term (the 4th element in the 1st row in (8)). As the flux seen by a winding is responsible for the voltage induced in it (at a fixed speed), the measured voltage seen by the voltage regulator (voltage in W1) can be modified with the *d*-axis current of W2 so as to increase or decrease the *d*-axis current commanded by the voltage regulator (reference setting for W1).

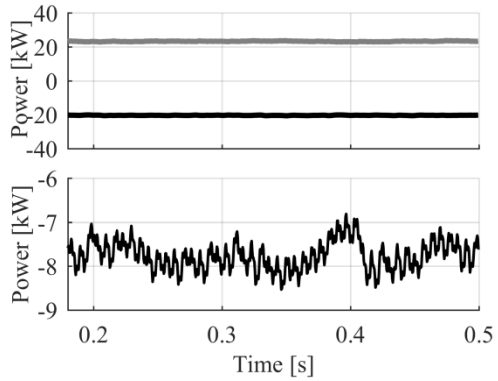

Fig. 8. Test of the machine at 300 rpm handling the total power of 43 kW. The top plot shows the power handled by each of the windings (black trace for W2 and grey for W1). The bottom plot shows the net power delivered to the grid (i.e. negative value of the total losses).

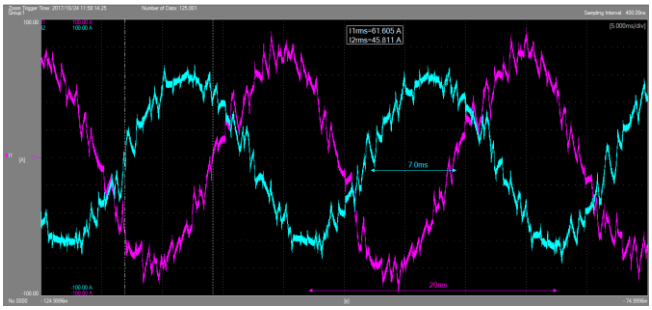

Fig. 9. Oscilloscope recording of the instantaneous currents in the two three-phase windings for operation at 50 Hz with peak *q*-axis current in W2 (green) equal to 60 A. Purple trace shows current in W1.

Fig. 10 illustrates phase *a* current in each of the two three-phase windings. The difference is now negligible, in contrast to Fig. 9. This ensures that the test conditions fully replicate the normal operating regimes of the machine.

Since W1 always operates in motoring, while W2 generates, the total losses can be evaluated as

$$\Delta P = \sum P_{\text{losses}} = P_{W1} - P_{W2} \quad (9)$$

It should be noted again that, since the loading dc machine could not be disconnected, the total losses in (9) include mechanical losses of both the tested machine and the loading machine; hence the resultant efficiency is somewhat lower than it would have been just for the tested machine itself.

As shown in [18, 19], if powers of the two windings W1 and W2 are measured and hence known, the efficiency can be evaluated using

$$\eta = \frac{(P_{W1} + P_{W2})/2}{P_{W1}} = 0.5\left(1 + \frac{P_{W2}}{P_{W1}}\right) \quad (10)$$

Measurements of W1 and W2 input/output powers were done at a fixed speed of rotation for a number of operating points, while varying the *q*-axis current of the generating (W2) winding. Considered speeds are in the stator frequency range 40 Hz to 70 Hz, with increment of 10 Hz. Winding W2 *q*-axis current is always varied from 0 A to 60 A peak, with an increment of 15 A.

Fig. 11 shows active powers in the motoring (W1) and generating (W2) windings, for the variation of the generating *q*-axis peak current in the range 0-60 A, at different operating frequencies (speeds) 40 to 70 Hz. As expected, active power variation in both windings is linear with respect to the generating winding *q*-axis current and also increases proportionally with speed.

Phase rms current in the windings W1 and W2 is illustrated in Fig. 12 for the same operating conditions as in Fig. 11. The currents in the two three-phase windings are equalised, so that the thermal conditions in all phases are the same as well, as already noted in conjunction with Fig. 10.

Equalisation of the W1 and W2 currents, shown in Fig. 12, is achieved by the described manipulation of W1 and W2 *d*-axis currents, which are shown in Fig. 13. For the frequencies between 40-60 Hz, the *d*-axis current should be the same for all the corresponding loading points since the voltage regulator increases stator voltage linearly with the speed (thus keeping stator flux constant). The differences observed in the currents in Figs. 12 and 13 at said frequencies are due to the progressive heating of the magnets that leads to a reduction in the rotor flux. This directly translates into a reduction of the negative *d*-axis current required to reach the same stator magnetic flux. At 70 Hz (more precisely, at 66 Hz), the voltage regulator hits the maximum stator voltage and the machine is further operated in the flux weakening region thus requiring higher values of negative *d*-axis current.

Finally, Fig. 14 shows total losses and efficiency, obtained using (9) and (10), with the speed as the parameter. As expected, efficiency of the machine is high in all operating points and it exceeds 95% in the normal operating region

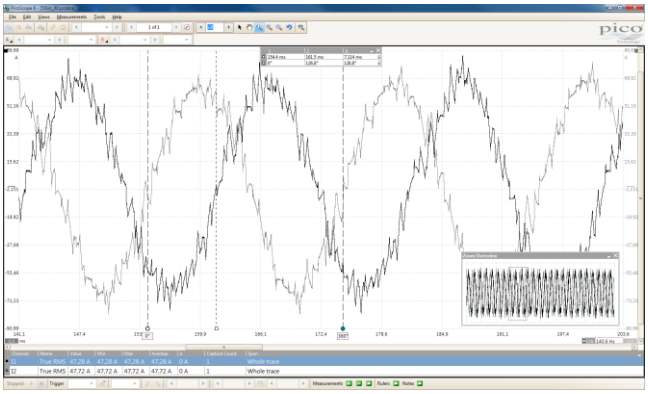

Fig. 10. Oscilloscope recording of the instantaneous currents in the two three-phase windings for operation at 50 Hz with peak q-axis current in W2 (black) equal to 60 A. Grey trace shows current in W1. The currents in the two windings have now been equalised.

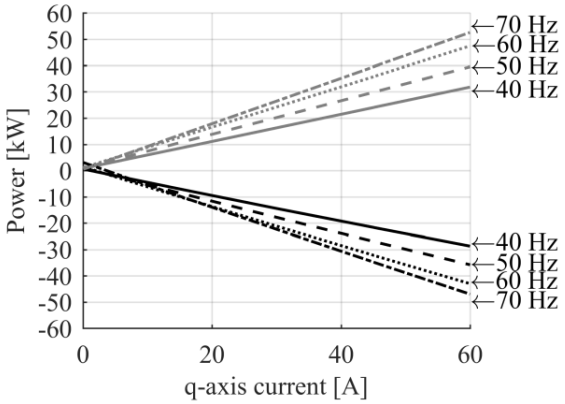

Fig. 11. Active powers of the motoring and generating windings (grey and black traces, respectively) as the peak q-axis current in the W2 is increased, at different rotational speeds. Solid trace is for 40, dashed for 50, dotted for 60 and dash-dotted for 70 Hz.

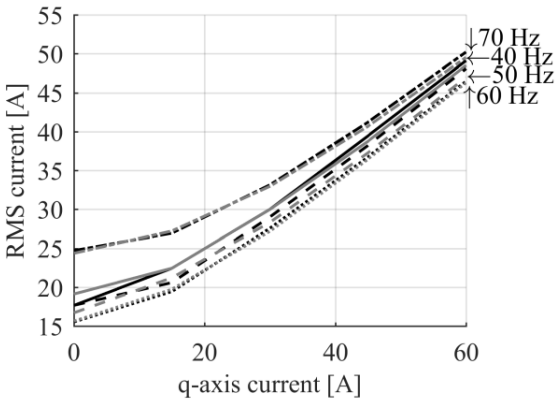

Fig. 12. Rms phase currents in W1 and W2 (grey and black traces, respectively), at different rotational speeds, against the peak q-axis current in the W2. Solid trace is for 40, dashed for 50, dotted for 60 and dash-dotted for 70 Hz.

(peak q-axis current above 30A) at practically all speeds of rotation. Total losses of course increase with the operating frequency (speed) due to an increase in both iron and mechanical losses. It has to be noted here once more that the total losses shown in Fig. 14 also include the mechanical losses of the dc loading machine.

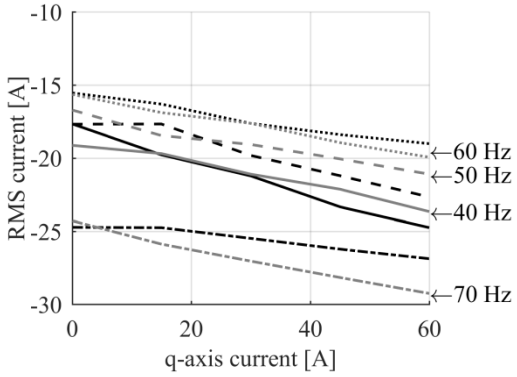

Fig. 13. Winding d-axis currents (rms values) in W1 and W2 (grey and black traces, respectively), at different rotational speeds, against the peak q-axis current in the W2. Solid trace is for 40, dashed for 50, dotted for 60 and dash-dotted for 70 Hz.

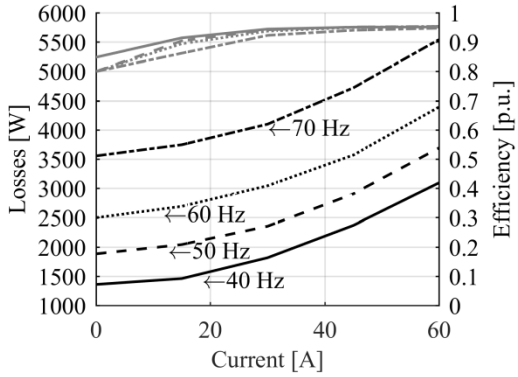

Fig. 14. Total losses of the machine (black traces) and efficiency (grey traces) against the q-axis current in the W2, at different rotational speeds. Solid trace is for 40, dashed for 50, dotted for 60 and dash-dotted for 70 Hz.

IV. Conclusion

A combined back-to-back/synthetic loading method is introduced for multiphase machines with multiple three-phase windings and near-sinusoidal winding distribution. This allows testing the machine/converter at up to full rated power without the need for additional equipment, such as a driving motor and converter, or a loading machine, and hence reduces the cost substantially.

Machine modelling and control are described for a six-phase permanent magnet machine and the method is then validated experimentally, using an industrial 150 kW laboratory rig. Illustrations of dynamics of the power sharing between the two three-phase windings are included, as are the results of the total loss evaluation and efficiency testing. A procedure that enables equalisation of the total rms current in the two windings is also described. The method is especially interesting in high-power machine/converter testing.

References

[1] J. P. McSharry, P. S. Hamer, D. Morrison, J. Nessa, and J. G. Rigsby, "Design, fabrication, back-to-back test of 14200-HP two-pole cylindrical rotor synchronous motor for ASD application," *IEEE Trans. Ind. Appl.*, vol. 34, no. 3, pp. 526–533, 1998.

[2] H. E. Jordan, J. H. Cook, and R. L. Smith, "Synthetic load testing of induction machines," *IEEE Trans. Power App. and Syst.*, vol. PAS-96, no. 4, pp. 1101-1104, 1977.

[3] I. Colak, S. Garvey, and T. M. Wright, "Mixed-frequency testing of induction machines using inverters," *5th European Conf. on Power Electronics and Applications EPE*, Brighton, UK, vol. 5, pp. 317-322, 1993.
[4] I. Colak, "Mixed-frequency testing of induction machines using inverters," *PhD Thesis*, University of Birmingham, Birmingham, UK, 1994.
[5] C. Grantham, H. Tabatabaei-Yazdi, and M. F. Rahman, "A novel method for rapid efficiency measurement of three phase induction motors," *IEEE Trans. Energy Conv.,* vol. 14, no. 4, pp. 1236-1240, 1999.
[6] J. Soltani, B. Szabados, and G. Hoolboom, "A new synthetic loading for large induction machines with no feedback into the power system," *IEEE Trans. Energy Conv*., vol. 17, no. 3, pp. 319-324, 2002.
[7] J. Soltani, B. Szabados, and G. Hoolboom, "A novel method of measurement of synchronous machine losses using synthetic loading," *IEEE Trans. Instr. and Measurement*, vol. 51, no. 6, pp. 1228-1233, 2002.
[8] A. Y. M. Abbas and J. E. Fletcher, "Synthetic loading applied to linear permanent magnet synchronous machines," *IET Renewable Power Generation*, vol. 4, no. 3, pp. 221–231, 2010.
[9] A. Y. M. Abbas and J. E. Fletcher, "The synthetic loading technique applied to the PM synchronous machine," *IEEE Trans. Energy Conv.,* vol. 26, no. 1, pp. 83-92, 2011.
[10] A. Y. M. Abbas and J. E. Fletcher, "The effect of direct axis current on the performance of the synthetic loading technique," *IEEE Trans. Energy Conv.,* vol. 26, no. 1, pp. 115-121, 2011.
[11] R. Bojoi, A. Tenconi, F. Profumo, and F. Farina, "Dual-source fed multi-phase induction motor drive for fuel cell vehicles: Topology and control," *Proc. IEEE Power Electronics Specialists Conference (PESC)*, Recife, Brazil, pp. 2676-2683, 2005.
[12] S. Rubino, R. Bojoi, A. Cavagnino, and S. Vaschetto, "Asymmetrical twelve-phase induction starter/generator for more electric engine aircraft," in *Proc. IEEE Energy Conv. Congress and Expo. ECCE,* Milwaukee, WI, USA, cd-rom (EC-0902), 2016.
[13] A. Tani, G. Serra, M. Mengoni, L. Zarri, G. Rini, and D. Casadei, "Dynamic stator current sharing in quadruple three-phase induction motor drives," in *Proc. IEEE Annual Conf. of the Ind. Electron. Soc. IECON*, Vienna, Austria, pp. 5173-5178, 2013.
[14] M. Mengoni, G. Sala, L. Zarri, A. Tani, G. Serra, Y. Gritli, and M. Duran, "Control of a fault-tolerant quadruple three-phase induction machine for more electric aircrafts," in *Proc. IEEE Annual Conf. of the Ind. Electron. Soc. IECON,* Firenze, Italy, pp. 5747-5753, 2016.
[15] I. Zoric, M. Jones, and E. Levi, "Arbitrary power sharing among three-phase winding sets of multiphase machines," *IEEE Trans. Ind. Electron*., vol. 65, no. 2, pp. 1128-1139, 2018.
[16] A. Galassini, A. Costabeber, C. Gerada, A. Tessarolo, and R. Menis, "Speed control with load sharing capabilities for multi-three phase synchronous motors," in *Proc. IEEE Annual Conf. of the Ind. Electron. Soc. IECON*, Beijing, PR China, pp. 4408-4413, 2017.
[17] M. J. Duran, I. Gonzalez-Prieto, H. Guzman, F. Barrero, and H. M. Kim, "Unbalanced operation of multiphase wind energy conversion systems connected to microgrids," in *Proc. IEEE Annual Conf. of the Ind. Electron. Soc. IECON*, Yokohama, Japan, pp. 1891-1896, 2015.
[18] F. Luise, S. Pieri, M. Mezzarobba, and A. Tessarolo, "Regenerative testing of a concentrated-winding permanent-magnet synchronous machine for offshore wind generation – Part I: Test concept and analysis," *IEEE Trans. Ind. Appl.,* vol. 48, no. 6, pp. 1779-1790, 2012.
[19] F. Luise, S. Pieri, M. Mezzarobba, and A. Tessarolo, "Regenerative testing of a concentrated-winding permanent-magnet synchronous machine for offshore wind generation – Part II: Test implementation and results," *IEEE Trans. Ind. Appl.,* vol. 48, no. 6, pp. 1791-1796, 2012.
[20] L. De Camillis, M. Matuonto, A Monti, and A Vignati, "Optimizing current control performance in double winding asynchronous motors in large power inverter drives," *IEEE Trans. on Power Electronics*, vol. 16, no. 5, pp. 676-685, 2001.
[21] M. Zabaleta, M. Jones, and E. Levi, "A tuning procedure for the current regulator loops in multiple three phase permanent magnet machines with low switching to fundamental frequency ratio," in *Proc. 19th European Conference on Power Electronics and Applications EPE-ECCE Europe*, Warsaw, Poland, pp. 1-10, 2017.
[22] M. Zabaleta, E. Levi, and M. Jones, "Dual three-phase PM generator parameter identification using experimental and simulated system responses," in *Proc. 19th Int. Symp. Power Electronics Ee*, Novi Sad, Serbia, pp. 1-6, 2017.

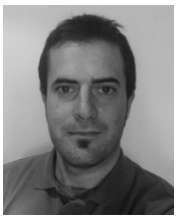

Mikel Zabaleta received his M.Sc. degree in industrial engineering from the Public University of Navarre, Pamplona, Spain, in 2004. He is currently working towards his PhD degree at the Liverpool John Moores University, UK.

He joined Ingeteam Power Technology, Pamplona, Spain in 2005. Since 2010, he has been working as the product manager for medium voltage converters in the wind power department, and is currently in charge of the development of the converter family for 3.3 kVac applications. His research interests are in the fields of multilevel converters, multiphase machines modelling and control, synchronous modulations and low switching frequency applications

Emil Levi (S'89, M'92, SM'99, F'09) received his MSc and the PhD degrees in Electrical Engineering from the University of Belgrade, Yugoslavia in 1986 and 1990, respectively. He joined Liverpool John Moores University, UK in May 1992 and is since September 2000 Professor of Electric Machines and Drives. He served as a Co-Editor-in-Chief of the IEEE Trans. on Industrial Electronics in the 2009-2013 period and is currently Editor-in-Chief of the IET Electric Power Applications and an Editor of the IEEE Trans. on Energy Conversion. He is the recipient of the Cyril Veinott award of the IEEE Power and Energy Society for 2009 and the Best Paper award of the IEEE Trans. on Industrial Electronics for 2008. In 2014 he received the "Outstanding Achievement Award" from the European Power Electronics (EPE) Association.

Martin Jones received his BEng degree (First Class Honours) in Electrical Engineering from the Liverpool John Moores University, UK in 2001. He was a research student at the Liverpool John Moores University from September 2001 till Spring 2005, when he received his PhD degree in Electrical Engineering. Dr Jones was a recipient of the IEE Robinson Research Scholarship for his PhD studies and is currently with Liverpool John Moores University as a Reader. His research is in the area of high performance ac drives.